Icarus 353 (2021) 113598

Contents lists available at ScienceDirect

Icarus

journal homepage: www.elsevier.com/locate/icarus

Impact of gradients at the martian terminator on the retrieval of ozone from SPICAM/MEx

A. Piccialli [a,*], A.C. Vandaele [a], L. Trompet [a], L. Neary [a], S. Viscardy [a], J.T. Erwin [a], A. Määttänen [b], F. Daerden [a], Y. Willame [a], S. Robert [a], S. Aoki [a], V. Wilquet [a], F. Lefèvre [b], F. Montmessin [c]

[a] Planetary Aeronomy, Royal Belgian Institute for Space Aeronomy, 3 av. Circulaire, B-1180 Brussels, Belgium
[b] LATMOS/IPSL, Sorbonne Université, UVSQ, CNRS, Paris, France
[c] LATMOS/IPSL, UVSQ Université Paris-Saclay, Sorbonne université, CNRS, Guyancourt, France

ARTICLE INFO

Keywords:
Mars
Atmosphere
Occultations
Ultraviolet observations
Radiative transfer
Photochemistry

ABSTRACT

Rapid variations of pressure, temperature and illumination at the day–night terminator have the potential to cause asymmetries in the abundance distribution of the atmosphere constituents along the line of sight (LOS) of a solar occultation experiment. Ozone, in particular, displays steep density gradients across the terminator of Mars due to photolysis. Nowadays, most of the retrieval algorithms for solar and stellar occultations rely on the assumption of a spherically symmetrical atmosphere. However, photochemically induced variations near sunrise/sunset conditions need to be taken into account in the retrieval technique in order to prevent inaccuracies.

We investigated the impact of gradients along the LOS of the solar occultation experiment SPICAM/Mars Express for the retrieval of ozone under sunrise/sunset conditions. In order to test the impact of different gradients, we selected four occultations at sunrise and at sunset each. Sunset occultations are located near the equator, while sunrise observations are situated at high latitudes in the South, because of the geometry of the orbit.

We used the diurnal variations in the ozone concentration obtained from a three-dimensional General Circulation Model (GEM-Mars) together with an adapted radiative transfer code (ASIMUT). The General Circulation Model (GCM) suggests that ozone variations strongly depend on latitude, altitude, and season. As shown by the model, near the equator and below 25 km, ozone changes only slightly with local time. Around 45 km, the density changes by several orders of magnitude across the terminator. At high latitudes in the South, during northern winter time, ozone variations at the terminator are negligible.

The impact of gradients on ozone retrievals is strongly related to the local atmospheric structure as predicted by the GCM. Sunset ozone retrievals are smaller than retrievals obtained assuming a spherically symmetrical atmosphere, with a maximum change of about 20%. At sunrise, the impact of gradients on the retrievals is negligible. This behavior can be explained by the specific geometry of sunrise observations, all situated at high latitudes in the South.

1. Introduction

Occultation, both solar and stellar, is a powerful technique to measure the vertical distribution of trace gases in planetary atmospheres. The major advantages of this technique are its high vertical resolution and its self-calibration mode. While stellar occultations probe the atmosphere preferably at night time, solar occultation are restricted to the terminator (Bertaux et al., 2006).

The atmosphere of a terrestrial planet at the day–night terminator is a region of great interest characterized by gradients of density and temperature, driven by differences in the solar illumination, and by

* Corresponding author.
E-mail addresses: arianna.piccialli@aeronomie.be (A. Piccialli), A-C.Vandaele@aeronomie.be (A.C. Vandaele), Loic.Trompet@aeronomie.be (L. Trompet), Lori.Neary@aeronomie.be (L. Neary), Sebastien.Viscardy@aeronomie.be (S. Viscardy), justin-tyler.erwin@aeronomie.be (J.T. Erwin), anni.maattanen@latmos.ipsl.fr (A. Määttänen), Frank.Daerden@aeronomie.be (F. Daerden), yannick.willame@aeronomie.be (Y. Willame), Severine.Robert@aeronomie.be (S. Robert), Shohei.Aoki@aeronomie.be (S. Aoki), Valerie.Wilquet@aeronomie.be (V. Wilquet), franck.lefevre@latmos.ipsl.fr (F. Lefèvre), franck.montmessin@latmos.ipsl.fr (F. Montmessin).

https://doi.org/10.1016/j.icarus.2019.113598
Received 22 April 2019; Received in revised form 22 October 2019; Accepted 6 December 2019
Available online 19 December 2019

sharp transitions in the chemical regime. Rapid variations in species concentration at the terminator have the potential to cause asymmetries in the species distributions along the line of sight (LOS) of a solar occultation experiment. Ozone, in particular, displays rapid changes due to photolysis more pronounced on the day side than on the night side (Natarajan et al., 2005; Lefèvre et al., 2004). Nowadays, most of the retrieval algorithms for solar and stellar occultations rely on the assumption of a spherically symmetrical atmosphere (Vandaele et al., 2006; Quémerais et al., 2006). However, photochemically induced variations near sunrise/sunset conditions need to be taken into account in the retrieval process in order to prevent inaccuracies (Boughner et al., 1980; Natarajan et al., 2005). In order to handle concentration gradients along the line of sight it is necessary to improve the retrieval schemes used to analyze occultation observations.

In the present paper, we test an improved retrieval scheme that handles different gradients along the line of sight and we focus in particular on the retrieval of ozone from SPICAM/Mars Express solar occultations taking into account variations in the temperature and in the ozone concentration at the day/night terminator. Ozone is a species with a short chemical lifetime and characterized by sharp gradients at the day–night terminator both on Earth and on Mars. On Mars, 3D General Circulation Models (GCMs) predict the existence of two ozone layers (Lefèvre et al., 2004; Daerden et al., 2019), instead of just one layer as on Earth. This was confirmed by SPICAM stellar occultations (Lebonnois et al., 2006), which revealed their existence on the nightside. The first layer is located below 30 km, and the second one – seasonally and spatially variable – is situated at higher altitudes between 30 and 60 km. While the lower layer displays only a weak diurnal cycle, the upper layer is strongly depleted by ultraviolet radiation at sunrise. It reappears as the Sun sets due to the recombination of O and O_2.

Previous observations reported that the largest ozone quantities are observed at high latitudes in the winter hemisphere where water vapor has condensed on the polar cap (Lebonnois et al., 2006; Willame et al., 2017). This was expected since ozone is anti-correlated to water vapor. Lower quantities of ozone are found at low latitudes and in the summer hemisphere (Lefèvre et al., 2004; Daerden et al., 2019).

We briefly describe the SPICAM-UV solar occultation dataset in Section 2. The GCM used as an input for this study is presented in Section 3. We review the retrieval technique in Section 4 and then present the results in Sections 5–7.

2. SPICAM-UV solar occultation dataset

SPICAM (SPectroscopie pour l'Investigation des Caractéristiques Atmosphériques de Mars), on board the ESA's mission Mars Express, is a remote sensing spectrometer observing in the ultraviolet (118–320 nm) and in the near infrared (1 – 1.7 μm). A detailed description of the instrument as well as its scientific objectives can be found in Bertaux et al. (2006). In the solar occultation mode, the UV instrument is used to measure the vertical profiles of O_3 and aerosols of the Martian atmosphere (Määttänen et al., 2013). During a solar occultation, the instrument points through the atmosphere toward the Sun as it rises or sets. When the instrument's line of sight to the Sun intersects the atmosphere, the solar light is absorbed by the atmospheric constituents (Quémerais et al., 2006; Montmessin et al., 2006; Forget et al., 2009; Lebonnois et al., 2006). A reference solar spectrum is obtained by recording the solar light above the dense part of the atmosphere (above 120 km). The ultraviolet sensor of SPICAM has a spectral resolution of 0.51 nm. The vertical sampling resolution obtained in solar occultation is less than 1 km.

Fig. 1 displays transmission spectra obtained at different altitudes for the observation 00633A02. The signal below 200 nm has a poor signal-to-noise ratio (SNR) due to the low emission of the Sun at those wavelengths and is not used in the retrievals. The ozone absorption band (Hartley band) is clearly visible around 250 nm. The

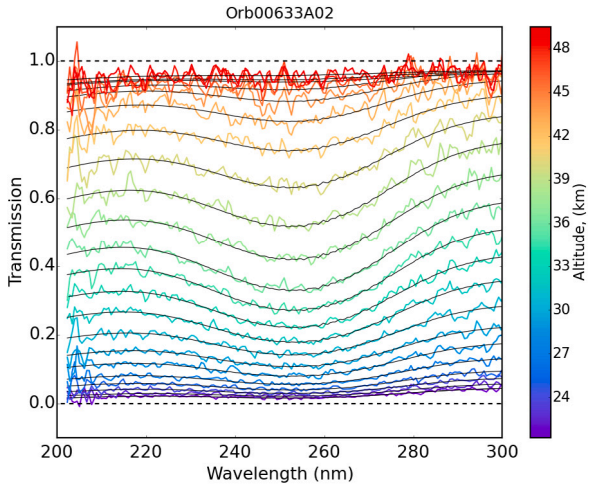

Fig. 1. Example of SPICAM transmission spectra at different altitudes: (blue) low altitudes; (red) high altitudes. Black lines are fitted spectra calculated using the radiative transfer code ASIMUT. (For interpretation of the references to color in this figure legend, the reader is referred to the web version of this article.)

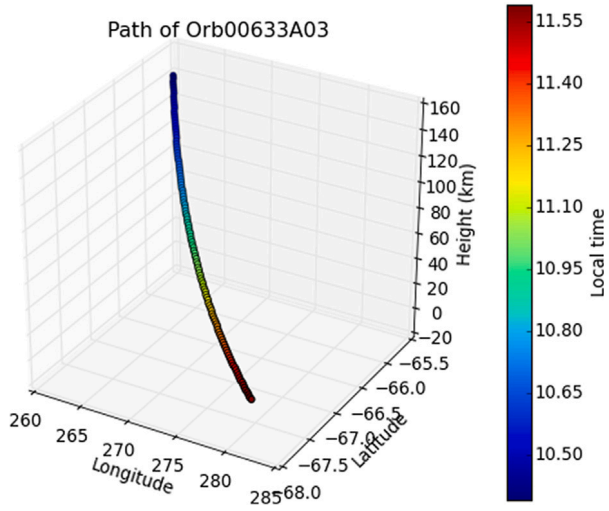

Fig. 2. Example of path described by the tangent point during an occultation (#00633A03). The colorbar shows the local time (hr) variation along the path. (For interpretation of the references to color in this figure legend, the reader is referred to the web version of this article.)

aerosols affect the entire spectral range by attenuating the spectrum approximately uniformly (Montmessin et al., 2006).

The reference location for each occultation is determined at the surface (see Fig. 2). However, the relative motion of the source often means that the locus of tangent points is far from vertical, leading to 'slanted' profiles, extending over several hundred kilometers horizontally. A solar occultation profile is then spread over a latitude and longitude interval, usually smaller than 20°. The local time of the tangent point is also changing at each altitude during an occultation. The spread of the occultation profile is larger close to the poles and decreases approaching the equator.

For this study we analyzed data from eight solar occultations acquired by SPICAM-UV between June and August 2004 (MY27) both at sunrise and at sunset (see Table 1). We selected only occultations acquired before June 2005 in order to avoid the oscillations caused by the MARSIS/MEx antenna (Määttänen et al., 2013). Due to such a constraint, there is a clear bias in the geolocalization of sunrise and sunset occultations: all sunset occultations are located near the equator while sunrise occultations are situated at high latitudes.

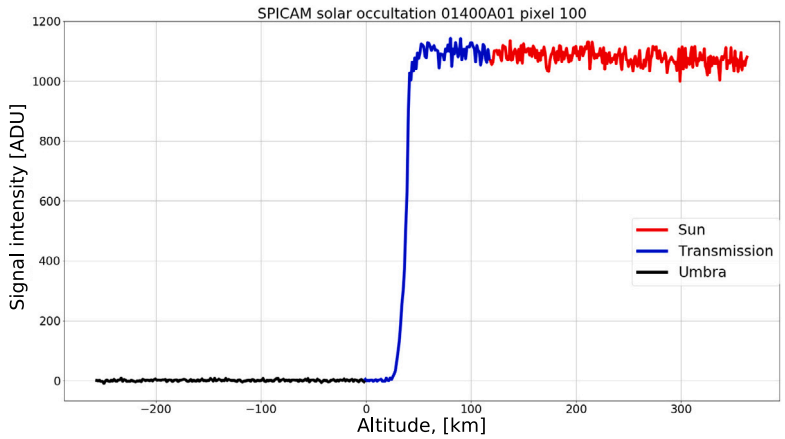

Fig. 3. Example of intensity of the signal recorded on one pixel of the detector. The "Sun" region lies above 120 km (red), the "Transmission" region between 0 and 120 km (blue) and the "Umbra" region under about 15 km of tangent altitude (black). (For interpretation of the references to color in this figure legend, the reader is referred to the web version of this article.)

Table 1
Solar occultations analyzed in this study. The reference location for each profile is determined at the surface. Ls is the solar longitude.

Occultation	Longitude	Latitude	Ls	Local time	Terminator
00472A02	342.76	−9.23	42.37	17.82	Sunset
00584A02	143.05	−18.02	56.27	17.52	Sunset
00633A02	10.80	−21.67	62.29	17.37	Sunset
00655A01	10.25	−23.46	64.99	17.30	Sunset
00584A03	47.56	−68.94	56.28	11.44	Sunrise
00633A03	280.26	−67.62	62.30	11.59	Sunrise
00642A02	117.83	−67.42	63.40	11.65	Sunrise
00682A02	157.93	−66.46	68.30	12.05	Sunrise

2.1. Transmittance estimation

The spectra recorded during a solar occultation measurement can be separated in three regions represented on Fig. 3:

- The "Sun" region: it contains solar spectra recorded when the LOS does not cross the atmosphere,
- The "Transmission" region: it contains atmospheric spectra recorded when the LOS crosses the atmosphere,
- The "Umbra" region: it contains the data recorded when all the light of the Sun has been absorbed or occulted by Mars.

For the Martian atmosphere, and given the SNR of SPICAM-UV, we consider that the separation between the "Sun" and the "Transmission" region occurs at 120 km of tangent altitude.

The solar reference spectrum S is computed by extrapolating, for each pixel, the intensity of the spectra recorded in the "Sun" region using a linear regression. Transmittances Tr are, then, computed by dividing the spectra of the "Transmission" region by the extrapolated solar reference spectrum S at the same time, i.e. at the same tangent altitude (in occultation measurements, each spectrum has a particular time of measurement and tangent altitude and they are proportional or inversely proportional for egress or ingress measurement, respectively). The noise δTr on the transmittances is calculated using the formula from Vandaele et al. (2013), and the SNR is the ratio of the transmittance Tr to the corresponding noise δTr:

$$\delta P(t) = \delta U + \sqrt{Tr(t)}(\delta S - \delta U) \tag{1a}$$

$$\delta Tr(t) = \frac{\sqrt{\delta P(t)^2 + Tr(t)^2 \delta S^2}}{S(t)} \tag{1b}$$

$$SNR(t) = \frac{Tr(t)}{\delta Tr(t)} \tag{1c}$$

where δS and δU are the noise in the "Sun" region and in the "Umbra" region respectively. They are computed for each pixel by taking the standard deviation of the signal in the corresponding region. δP is the noise for the "Transmission" region in unit of ADU (Analog-to-Digital units).

In a perfect measurement, the LOS of the instrument does not move on the Sun, and the detector sensitivity remains constant, so that we would expect the signal to be constant in the "Sun" region within the noise. In practice, this is not always the case, and taking into account all the spectra recorded in the "Sun" region may not lead to the correct extrapolated solar spectra. To take into account a variation of the signal along the occultation, we use a simple linear regression on the signal of each pixel in the Sun region, in order to extrapolate a solar reference spectrum for each spectrum in the transmission region.

We have adapted the algorithm used for SOIR (Nevejans et al., 2006) on Venus Express and described in Trompet et al. (2016). This algorithm is based on the fact that we expect that the transmittances Tr will not deviate too much from 1.0 for the highest tangent altitudes, i.e. when the solar light is still too weakly absorbed to be seen on the spectra. Concretely, we expect that the estimated transmittances do not deviate further than n times the values of the noise δTr : $Tr - n * \delta Tr < 1 < Tr + n * \delta Tr$, where n is in the range $[1, 3]$.

The value n is not fixed and a loop over that value has been added as the dataset can be rapidly treated. The value n begins with the value of 1 and increases by step of 0.5 if the criteria (Eq. (1c)) are not satisfied until the value of 3.

During the acquisition of a spectrum, the signal is spread on several spatial lines of the detector. For SPICAM, the signal on these different lines are binned into five bands.

For this study, these five bands have been added up to enhance the SNR ratio of the calibrated spectra. Using the five bands, we noticed an increase of the mean SNR over the whole dataset of 30% with respect to the case where only the three middle bands were taken and of 67% with respect to the case where only the middle band was used.

3. Model fields of atmospheric quantities

We use the GEM-Mars three-dimensional General Circulation Model (GEM-Mars GCM) with online chemistry (meaning photolysis and reaction rates, production and loss rates are computed at each model integration step) for the atmospheric input profiles and to quantify the gradients across the terminator. The model includes gas-phase photochemistry (46 reactions in total), parameterizations for molecular diffusion, CO_2 condensation/sublimation and pressure cycle, water cycle with cloud radiative feedbacks, non-condensable gas enrichment, and a dust lifting scheme for saltation and dust devils. The gas-phase species,

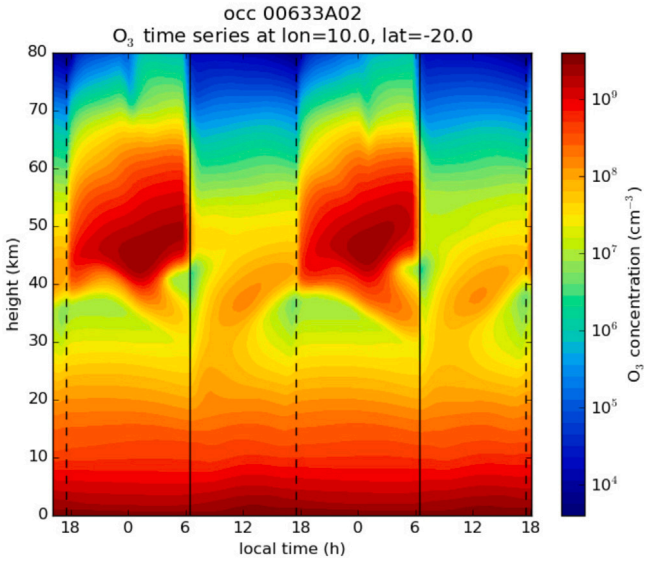

Fig. 4. Time series profile of ozone concentration for one GCM model point at the time and location of the SPICAM occultation #00633A02 (solar longitude: 62.3°). The solid (dotted) vertical line represents the sunrise (sunset) terminator. (For interpretation of the references to color in this figure legend, the reader is referred to the web version of this article.)

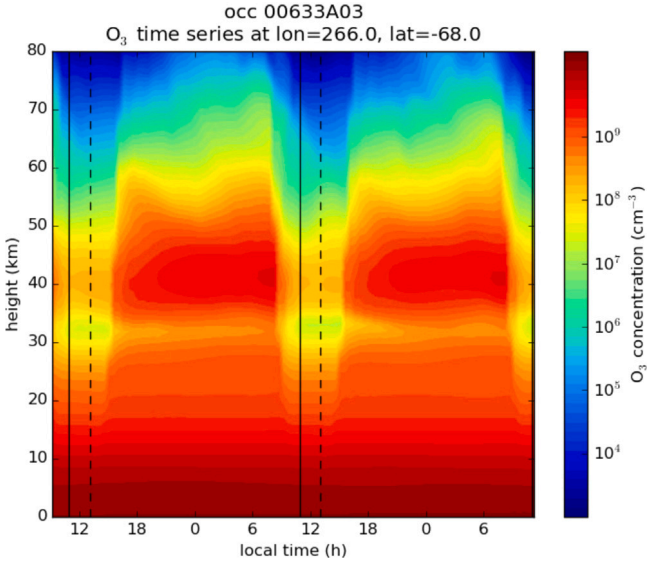

Fig. 5. Time series profile of ozone concentration for one GCM model point at the time and location of the SPICAM occultation #00633A03 (solar longitude: 62.3°). The solid (dotted) vertical line represents the sunrise (sunset) terminator. (For interpretation of the references to color in this figure legend, the reader is referred to the web version of this article.)

dust and water ice particles are advected using the semi-Lagrangian dynamical core.

The photolysis and reaction rates are calculated at each model integration time step, and absorption by CO_2, O_2, O_3, H_2O and H_2O_2 along the line of sight as well as attenuation by dust and water ice are taken into account.

A detailed description and evaluation of the model can be found in Neary and Daerden (2018) with further information regarding the chemistry in Daerden et al. (2019).

To provide input profiles, the model was run at a horizontal resolution of $4° \times 4°$ (approximately 237 km longitudinal spacing at the equator) and 103 unevenly spaced vertical levels from the surface up to $\sim$ 150 km. The spacing of levels near the surface is of the order of meters, increasing to $\sim$ 1 km in the $10 - 50$ km altitude range. A simulation was performed for a generic Mars year with average dust loading (not year specific) resulting from the dust-lifting scheme in the model with orbital parameters set to MY 28. The dynamical and chemical integration timestep was 1/48th of a Mars sol ($\sim$ 30 min).

For the gradients, profiles of temperature and ozone were provided at each model timestep for the period 2 h before until 2 h after sunrise/sunset for each grid point the occultation traversed.

Below 25 km, the gradients at both sunrise and sunset terminators are not large, but above this altitude, and in particular at $\sim$ 45 km near the equator, the density changes by several orders of magnitude across the terminator (See Figs. 4, and 6). At sunrise, photolysis of ozone occurs, as seen by its rapid depletion. There is some transport out of the boundary layer above 30 km during the afternoon. At sunset, photolysis stops and the ozone builds up due to the recombination of O and O_2 in the presence of CO_2. There is also a signature of downward transport during the night before sunrise. At southern high latitudes, during the winter, ozone variations at the terminator are almost negligible (Figs. 5 and 6 left).

4. Retrieval method description

4.1. Simulation

All retrievals of the spectra have been performed using the ASIMUT-ALVL radiative code developed at IASB-BIRA (Vandaele et al., 2006). Initially developed for Earth observation missions (IASI and ACE-FTS, Vandenbussche et al. (2013)), the code was later adapted for planetary atmospheres, in particular for Venus (Vandaele et al., 2008) and Mars (Drummond et al., 2011; Robert et al., 2017, 2016; Vandaele et al., 2018). ASIMUT-ALVL is a modular program for radiative transfer calculations in planetary atmospheres. This code was developed with the objective to be as general as possible, accepting different instrument types (Fourier Transform Spectrometers, grating spectrometers, AOTF combined with an echelle grating) and different viewing geometries (nadir, ground-based, solar occultation/limb). Different radiation contributions are taken into account: direct Sun or reflected on the surface, surface emission and thermal atmospheric emission. Spectra can be simulated/retrieved in the IR, the visible, and in the UV as well. The surface is considered by default to be Lambertian, but a more complex treatment is possible. The determination of the radiation path through the atmosphere, i.e. the path followed by the radiation reaching the instrument, requires that the planet's curvature and refraction are taken into account. The model is based on the ray-tracing program FSCATM (Gallery et al., 1983). ASIMUT-ALVL has been coupled to SPHER/TMATRIX (Mishchenko and Travis, 1998) and LIDORT (Spurr, 2006) codes (Kochenova et al., 2011) to include the complete treatment of the scattering effects into the radiative transfer calculations. Aerosols are included in the ASIMUT-ALVL code, either through extinction only (ASIMUT) or considering their scattering properties (ALVL, through the call to LIDORT). The main retrieval module is based on the Optimal Estimation Method (Rodgers, 2000) coupled to the analytical calculation of the Jacobians. It enables simultaneous or sequential fitting of different parts of one or more spectra, in order to retrieve the surface temperature, columns or vertical profiles for molecular species or for aerosols and to fully characterize the outputs (averaging kernels, errors, DOFS, etc.). The model assumes a one-dimensional atmosphere, with all parameters varying only with the vertical variable, the altitude. More detailed information regarding the retrieval process and the uncertainties calculation can be found in Appendix.

In this work, ASIMUT has been used without calling LIDORT since scattering by the atmosphere was considered negligible in solar occultation. All spectra of one occultation observation are analyzed simultaneously (all transmittances at the various tangent heights) by ASIMUT, which derives one single O_3 profile to best fit the ensemble

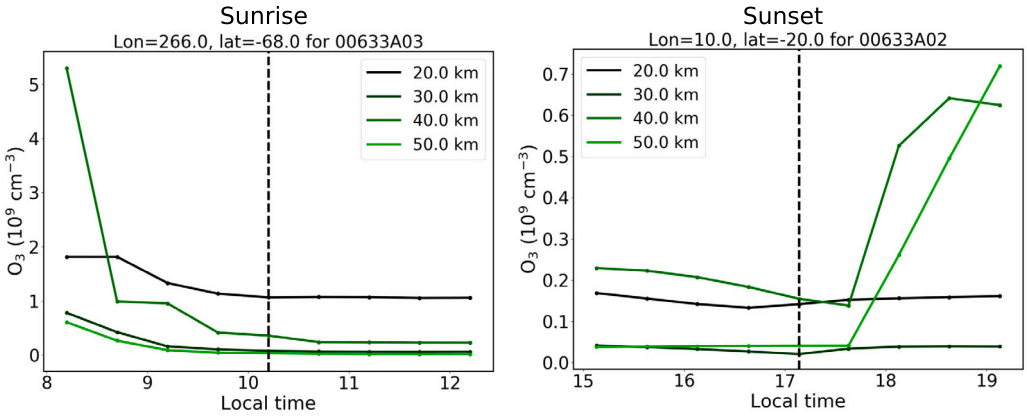

Fig. 6. The diurnal variation in the model ozone at sunrise (occultation 00633A03) and at sunset (occultation 00633A02) for different altitudes. The dashed line shows the local time of the terminator.

of spectra. The atmosphere was structured in layers whose boundaries were the different tangent altitudes of the observation, adding layers of 1.5 km width above the highest tangent height up to 125.0 km, which was considered the upper limit. Aerosols were not taken in account into the retrieval procedure. ASIMUT enables the user to fit the baseline spectrum. By configuring this additional fit, impact due to the uncertainties concerning aerosols could be reduced.

The equation describing the radiative transfer through the atmosphere (when no scattering is present) can be written as:

$$I(\nu) = I_0(\nu)e^{-\tau(\nu,0,z)} + \int_0^z B(\nu, T(s))\alpha(\nu, s)e^{-\tau(\nu,0,z)}ds \tag{2}$$

where I_0 represents the light intensity at the starting point of the ray path situated at the distance z from the observer, $\alpha(\nu, s)$ is the absorption coefficient, $B(\nu, T)$ is the Planck function, and

$$\tau(\nu, s_1, s_2) = \int_{s_1}^{s_2} \alpha(\nu, s)ds \tag{3}$$

is the optical depth along the path between the points s_1 and s_2. The integration in Eq. (2) occurs along the LOS. The ray tracing (i.e. the determination of the atmosphere characteristics along the LOS) is done by integrating the temperature, the pressure, the total density, and the partial densities of all atmospheric constituents in the Curtis–Godson approximation (Goody, 1952; Godson, 1953). Under this approximation the effective pressure ($P^\star$), the temperature ($T^\star$), and the density of species k ($N_k^\star$) needed to calculate the optical depth in a layer can be obtained by:

$$P^\star = \frac{\int P \cdot \rho \cdot ds}{\int \rho \cdot ds} \tag{4}$$

$$T^\star = \frac{\int T \cdot \rho \cdot ds}{\int \rho \cdot ds} \tag{5}$$

$$N_k^\star = \frac{\int N_k \cdot \rho \cdot ds}{\int \rho \cdot ds} \tag{6}$$

where ρ is the total air density, P, T, and N_k are respectively the pressure, the temperature, and the density of species k within the layer, and ds is the elementary path length through the layer on which the integration is done. The calculation of the integral is performed on a sub-grid of layers separated by 200 m.

The optical depth in each of the layers are calculated considering absorption/extinction by O_3, CO_2 and Rayleigh scattering. For CO_2, the cross-sections from Huestis and Berkowitz (2010) have been selected since they cover a wide spectral interval at relatively high resolution. They are in very good agreement with the data of Parkinson et al. (2003) obtained at 295 K. O_3 cross-sections have been built around the temperature dependent data sets of Serdyuchenko et al. (2014), extending the cross sections towards the shorter wavelength by using either the Reims data set (Brion et al., 1993; Daumont et al., 1992; Malicet et al., 1995) or the JPL compilation (Sander et al., 2011) depending on the available temperatures. From these data, a temperature dependent cross-section was built for O_3 which was used to calculate the optical depth at the temperature of the layer. Rayleigh scattering was included only as an extinction (no true scattering effects considered) using the data from Sneep and Ubachs (2005). Transmittances corresponding to each sounded altitude were fitted by considering the absorption of all layers traversed by the LOS of the instrument. They were then convolved to correspond to the resolution of the SPICAM instrument (0.51 nm).

4.2. Gradients as variation along the LOS

The treatment of solar occultation observation has been improved in this work by considering gradients and variations of the density and temperature along the LOS and in particular at the terminator. Three different gradients can be considered: (1) Temperature gradients across the terminator; (2) (Total) density gradients across the terminator; and (3) Density variations along the LOS. These gradients will have an impact on the ray tracing procedure (more accurate determination of the temperature, pressure, and densities within the layers of the atmosphere) and on the optical depth of the species, since they depend on the temperature and the partial densities of the species.

The correction for the gradients consists of introducing a correction which depends on the top and bottom altitudes of the layer, which in fact correspond to slightly different Local Solar Times (LST_{bottom} and LST_{top}, see Fig. 7). Two calculations need to be done for the Day and Night sides respectively. Indeed, at the dawn terminator, the local solar time increases towards the day side and decreases towards the night side. At dusk, this behavior reverses..

$$LST_{b/t}^N = LST_{terminator} - f(A_{b/t}^z) \tag{7}$$

$$LST_{b/t}^D = LST_{terminator} + f(A_{b/t}^z) \tag{8}$$

where b and t stand for bottom and top respectively, A^z is the angle between the LOS and the line joining the point along the LOS at altitude z and the center of the planet and f is a function describing the link between A^z and time defined by the geometry of the observation.

In the following, we will introduce 'Day' and 'Night' densities or temperatures ($T_i^{\star D}$, $T_i^{\star N}$, $N_{k,i}^{\star D}$, $N_{k,i}^{\star N}$, for species k and layer i); these will in fact refer respectively to 'after' and 'before' the terminator (see Fig. 7).

The different gradients are implemented in the following way. When the user asks to take the temperature gradient into account, two optical depths are calculated for each layer, corresponding to the two 'Day' and 'Night' temperatures. These temperatures are calculated using Curtis–Godson approximation (Eq. (5)), where the temperature in the layer is

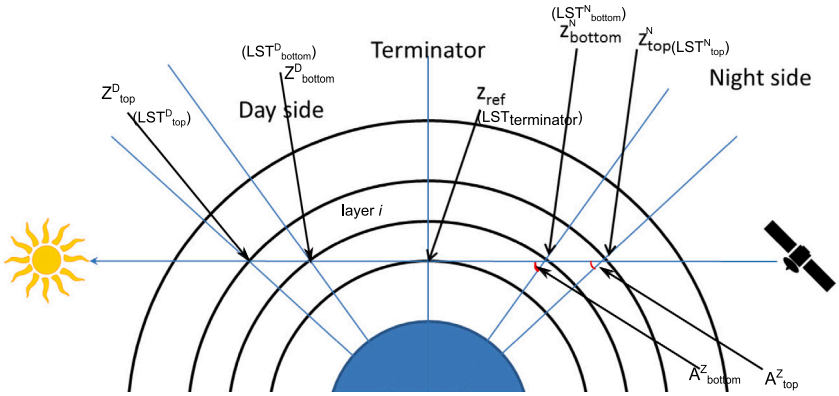

Fig. 7. Geometry of a solar occultation; definition of the 'Day' and 'Night' sides.

interpolated from the GEM-Mars simulation data at the LST corrected using Eqs. (7)–(8). Note that the calculation of the 'Night' optical depth is done only if the two temperatures differ by at least a minimum value which can be specified by the user (default value set to 2.0 K, minimal value = 0.1 K). Then, the total optical depth (OD) for the layer i and the species k is the average of the 'Day' and 'Night' side contributions:

$$OD_i^k = \frac{[OD_i^k(T_i^{\star D}) \times N_{k,i}^{\star D} + OD_i^k(T_i^{\star N}) \times N_{k,i}^{\star N}]}{2} \quad (9)$$

When the user asks to take into account gradients or variations of densities (total density or density of a specific species, such as O_3), the densities of the 'Day' and 'Night' side of the terminator are deduced using the Curtis–Godson approximation (Eq. (6)), based on interpolated values of the densities from GEM-Mars simulation data at the LST corrected using Eqs. (7)–(8)

4.3. Fit strategy

Several input parameters are needed to constrain the retrieval: *a priori* vertical profiles of the different species included (CO_2 and O_3) as well as of the temperature and pressure of the atmosphere. All a priori information is taken from the GEM-Mars simulations.

We assumed as an *a priori* nominal ozone profile the global average ozone VMR from GEM-Mars; i.e. average of all profiles at all Lat/Lon and seasons for one year (MY27). The mean and standard deviation of the ozone volume mixing ratio (VMR), in addition to mean temperature, pressure, and altitude, were derived from the GEM-Mars output of 48 time-steps per day and one day per 10 Ls, for a total of 1728 individual time-steps. The MOLA topographical surface height (Smith et al., 1999) was added to each vertical profile, so that the altitude coordinates are relative to the MGM1025 Mars areoid (Lemoine et al., 2001), and then each individual vertical profile was averaged into 1 km bins from −8 km to 165 km. The vertical profiles were weighted by spherical surface area of the latitude/longitude grid to not oversample the poles due to the regular grid, as well as weighted by the vertical extent of each altitude point to not oversample the near surface profiles due to the adaptive vertical grid. A more detailed description of this derivation, as well as the effects of different methods of averaging and weighting on the *a priori* profiles, will be discussed in a separate article in preparation (Erwin et al., 2018).

In a typical retrieval of an (solar) occultation observation, the altitudes at which the O_3 densities are retrieved are the different tangent heights of the different transmittances.

5. Ozone retrievals assuming a spherically symmetrical atmosphere

As a first step, we performed the retrieval of ozone assuming a spherically symmetrical atmosphere. Fig. 1 displays transmission spectra at different altitudes (see colorbar) compared to simulated spectra

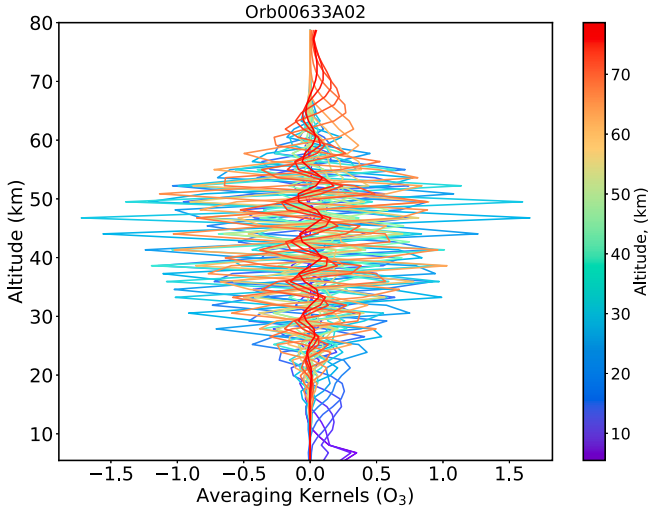

Fig. 8. Averaging kernels for occultation #00633A02.

(black solid line) for occultation #00633A02. In addition to the retrieved ozone profiles, ASIMUT produces several metrics that can be used to assess the retrievals. The averaging kernels are one of them. Averaging kernels allow to study how the information content is distributed in the retrieved profiles. They provide an estimation of the vertical sensitivity of the retrieval and peak at the altitude of maximum sensitivity. Fig. 8 shows the averaging kernel for occultation #00633A02. From this plot it is evident that the information content is constrained to the altitude range $\sim 20 - -60$ km. Below this altitude, the horizontal opacity of the dust limits the measurements.

We assessed the sensitivity of the ASIMUT ozone profile retrieval algorithm to a number of *a priori* assumptions. We studied the impact of the *a priori* ozone profiles, and of the initial temperature profile on the retrieved ozone profile, as described in more details below.

5.1. Sensitivity to the ozone a priori profile

We tested the dependency of ozone retrievals to the choice of the ozone *a priori* profile. We used three profiles as *a priori* obtained by multiplying the nominal *a priori* ozone profile by different factors. In Fig. 9 (top) we present two tests respectively for occultation #00633A02 at sunset and occultation #00633A03 at sunrise. Bottom panels in Fig. 9 are similar, but this time we used as *a priori* profiles constant VMR profiles. In all cases, the retrieved profiles converge within the expected uncertainty, except at low altitudes during sunrise.

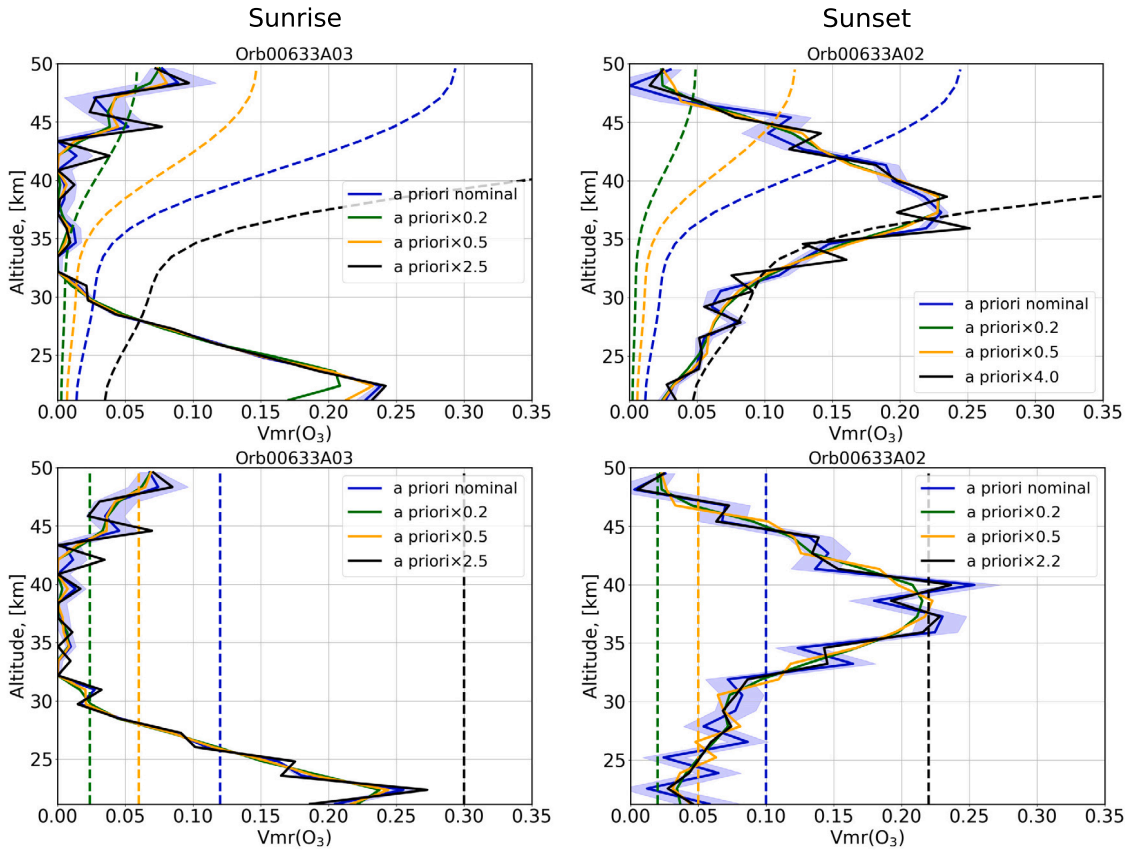

Fig. 9. Retrieved ozone profiles [ppm] (solid lines), starting from different first-guess profiles (dashed lines), for occultation #00633A03 (left panels) at sunrise and occultation #00633A02 (right panels) at sunset. Top panels use *a priori* profiles derived from the nominal *a priori* profile (dashed lines). Bottom panels use constant profiles as *a priori*.

5.2. Sensitivity to the temperature profile

We tested the sensitivity of the retrieved ozone profiles to the initial choice of temperature profile. We used as nominal temperature profile the global/temporal average temperature from GEM-Mars. We then tested two other temperature profiles obtained by adding ±15 K to the nominal profile. This value lies within the uncertainty on temperature in GEM-Mars (Neary and Daerden, 2018). We found a percentage change in the ozone profiles obtained using the two temperature profiles (blue and red lines in Fig. 10) smaller than 25% at 42 km.

5.3. Error analysis

Errors on the retrieved ozone result from random noise in the measurements and they are quantified in the inversion method. These random errors are < 5% between 30 and 40 km; < 10% below and above these altitudes and they reach a maximum value of 40% at the upper and lower boundaries. Another source of error on the retrieval of ozone profiles comes from the choice of *a priori* O_3 vmr profile. The retrieved ozone is particularly stable against a change in the *a priori* O_3 vmr profile (Fig. 9). However, uncertainties are mainly dominated by errors due to the initial temperature profile. A change in the input temperature profile produces a maximum difference of ±25% on ozone at 42 km (Fig. 10).

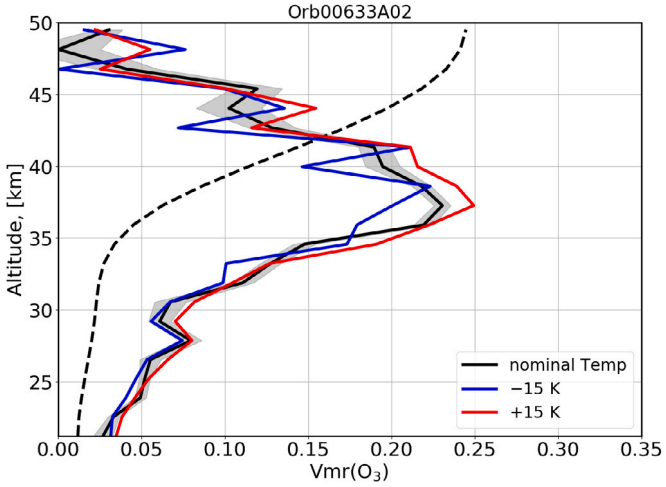

Fig. 10. Retrieved ozone profiles [ppm] obtained assuming different first-guess temperatures profiles: (black) nominal temperature; (blue) nominal-15 K; and (red) nominal+15 K. The gray area marks the uncertainty of the retrieved profile. For clarity, only the uncertainty for the nominal profile is shown, similar values are found for the other retrievals. The *a priori* profile (dashed line) is also shown. (For interpretation of the references to color in this figure legend, the reader is referred to the web version of this article.)

6. Ozone retrievals assuming concentration and temperature gradients around the terminator

6.1. Sensitivity to temperature gradients

We tested the sensitivity of retrievals to temperature and total density gradients provided by the GEM-Mars, described in Section 3. As mentioned in Section 4.2, if the difference in dayside and nightside temperatures exceeds a threshold, different densities are used for the day and night sides. This threshold is configurable. The default value is set to 2.0 K, we tested in addition a minimal value of 0.1 K. Moreover, we multiplied the GEM-Mars gradients by a factor of 2 and

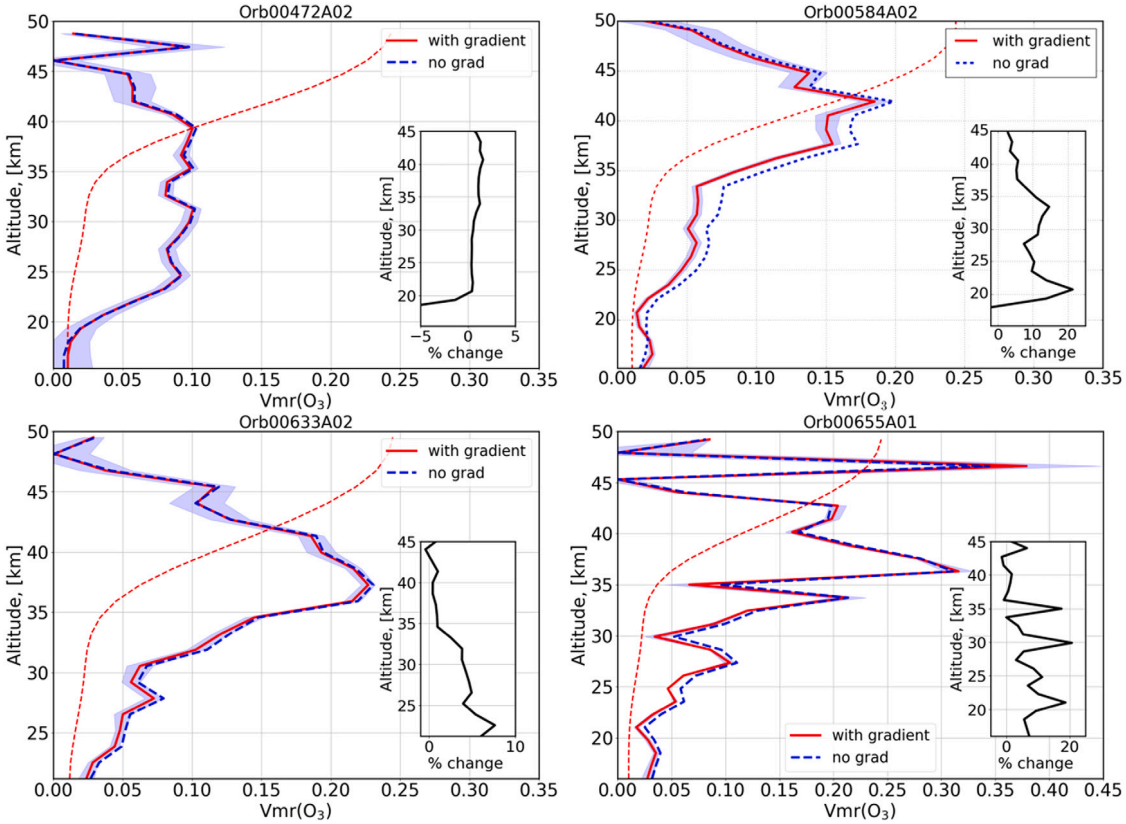

Fig. 11. Retrieved ozone profiles [ppm] for different occultations at sunset derived using GEM-Mars gradients (red solid lines) compared to profiles retrieved assuming a spherically symmetrical atmosphere (blue dashed lines). The *a priori* profile used for the retrieval is also shown (red dashed line). The insert panel shows the vmr difference in percent between the two retrievals.

5. Temperature gradients do not have any impact on the retrievals of ozone (figures are not shown here). This can be explained by the small temperature dependence of the O_3 cross sections. Nevertheless, we included temperature gradients in the retrieval process.

6.2. *Sensitivity to* O_3 *gradients*

We investigated the impact of taking into account the variations of ozone concentrations along the LOS at the day/night terminator. As input, we provided the ozone gradients calculated by the GEM-Mars (see Section 3). The differences in the model between the ozone variations for sunset and sunrise conditions, as well as for different locations (see Figs. 4 and 5), suggest that the effects of gradients on the retrievals should change for different occultations. The steeper gradient for the selected sunset occultations at low latitudes indicates the impact of gradients will be stronger for these occultations compared to sunrise data (Fig. 6).

Figs. 11 and 12 show retrieved ozone profiles for different occultations respectively at sunset and sunrise. Ozone profiles (solid red line) derived using GEM-Mars gradients are compared to profiles obtained assuming a spherically symmetrical atmosphere (blue dashed line). The insert panels show the vmr differences in percent between the two retrievals. At sunset (Fig. 11), retrievals show an ozone layer located in the altitude range 35 – −50 km. The inclusion of gradients in the retrieval method results in a $< 20\%$ reduction in ozone mixing ratio for sunset condition. Except for occultation #00584A02, the impact of retrievals lies within the error bar. The rapid variations observed for occultation #00655A01 are due to the retrieval procedure.

At sunrise (Fig. 12), profiles show the presence of an ozone layer located near the surface, the top of which is located at altitudes below 30 km. The impact of gradients on retrievals at sunrise is negligible. This behavior can be explained by the specific locations of sunrise occultations. In fact, as shown in Fig. 5, the day length is much shorter compared to the night at these latitudes and season and the ozone gradient is not very sharp.

In order to test the sensitivity of the retrievals on the initial ozone gradient, we multiplied the difference between day and night ozone along the LOS (provided by GEM-Mars) by factors of 2 and 3. Factors 1, 2, and 3 produce a percentage change with respect to the nominal profile of respectively: $< 7\%$, $< 30\%$, and $< 59\%$ at altitudes below 30 km (See Fig. 13).

The effect of gradients on the retrievals depends on the inputs gradients provided by the photochemical model, in our case GEM-Mars. The model gradients, moreover, strongly depend on the latitude, altitude, and season of the occultations, since ozone is dependent on all these factors.

7. Comparison to a different retrieval strategy

In order to validate different retrieval methods, we compared our results with the profiles of ozone from SPICAM solar occultations analyzed by Määttänen et al. (2013) (LATMOS retrievals from now on). It is important to notice that the spectral fitting strategy for LATMOS retrievals is different from the one applied in this study: LATMOS retrievals result in profiles of concentrations of ozone integrated along the LOS (slant profiles). ASIMUT provides both vertical and slant profiles. To compare the results obtained from the two methods, in this section we are therefore showing ASIMUT slant retrievals.

The data analysis method for the LATMOS retrievals are discussed in Quémerais et al. (2006), Montmessin et al. (2006), Määttänen et al. (2013) and are only briefly summarized here. The transmission spectra are calculated by averaging the solar spectrum measured above 120 km, and then dividing all the spectra by this reference spectrum. Only spectra void of spurious high-gain peaks or oscillations caused by the

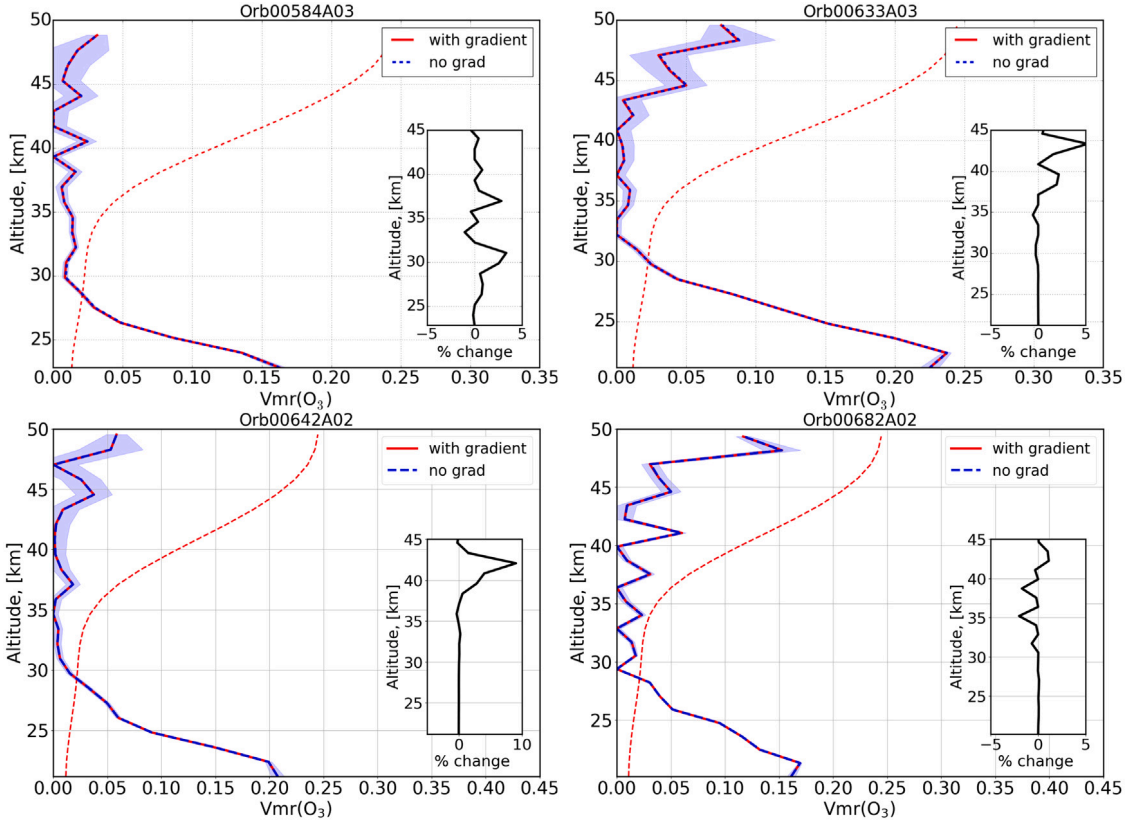

Fig. 12. As in Fig. 11 but for occultations acquired at sunrise.

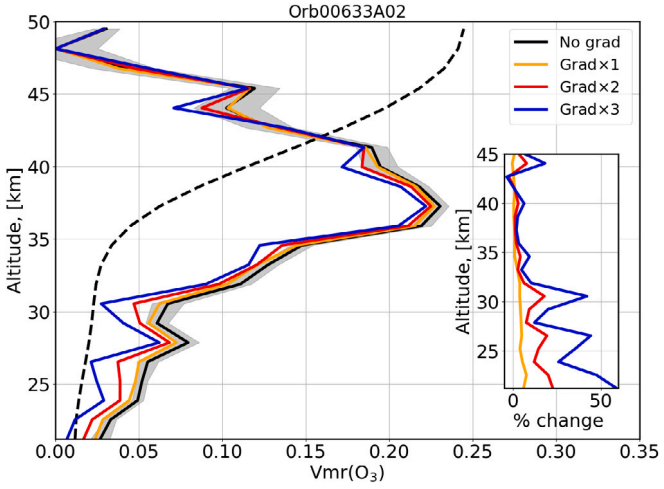

Fig. 13. Retrieved ozone profiles [ppm] for occultation #0633A02 derived using GEM-Mars gradients compared to the profile retrieved assuming a spherically symmetrical atmosphere (black line). GEM-Mars gradients were multiplied by different factors: 1 (yellow line), 2 (red line), and 3 (blue line). The *a priori* profile used for the retrieval is also shown (black dashed line). The insert panel shows the VMR difference in percent between the retrievals. (For interpretation of the references to color in this figure legend, the reader is referred to the web version of this article.)

MARSIS radar antennae are used in the procedure (see Määttänen et al. (2013)). To obtain the LOS ozone columns, the transmission spectra are fitted with a model based on the Beer–Lambert (BL) law that in this case describes the total absorption on the LOS by gases (CO_2, O_3) and by aerosols (using the so-called α-model: O'Neill and Royer (1993); Dubovik et al. (2000)). The BL model does not include any assumptions of gradients along the line of sight, since it simply describes the transmissions as the result of the sum of the extinctions caused by the total concentrations of species on the LOS. The BL model is fitted to the transmissions by using a Levenberg–Marquardt method (IDL routine MPFIT, Markwardt (2009)) and adjusting simultaneously the four unknowns: total concentrations of CO_2 and O_3, the dust optical depth and the α coefficient. As the fitting is started from the top of the atmosphere (transmission is essentially equal to one, so no absorption is expected) the *a priori* values for O_3 and dust are started from a very small value (practically zero) at the top of the atmosphere. Once the fitting procedure finds positive values for these variables, the fitting for each subsequent layer starts with the value of the previous layer as a first guess. Since the Sun is quite dim in the UV, the transmission spectra are very noisy within the CO_2 absorption band below 200 nm, often preventing the fitting routine from converging. We improved the CO_2 fits significantly by defining the *a priori* for CO_2 from profiles of the Mars Climate Database (MCD v4.3, Millour et al. (2008); see details in Määttänen et al. (2013)). The fitting provides LOS column concentrations of CO_2 and O_3, and LOS aerosol optical depth and a value for α, and the corresponding uncertainties (see Määttänen et al. (2013) for details on the error estimation).

Fig. 14 displays the comparison between ozone slant densities for three occultations at sunrise and sunset. Different colors correspond respectively to: (black) ASIMUT retrievals assuming a spherically symmetrical atmosphere; (red) ASIMUT retrievals including GEM-Mars gradients; and (orange) LATMOS retrievals assuming a spherically symmetrical atmosphere. The perfect agreement between ASIMUT retrievals assuming a spherically symmetrical atmosphere and ASIMUT retrievals including GEM-Mars gradients was expected, since gradients should not impact the LOS optical thickness. ASIMUT and LATMOS retrievals are in very good agreement. Differences, especially for sunset occultations, may be explained by different *a priori* inputs.

8. Summary

Rapid changes in the species concentration at the day–night terminator driven by differences in the solar illumination may cause asymmetries along the LOS of a solar occultation experiment that need to be

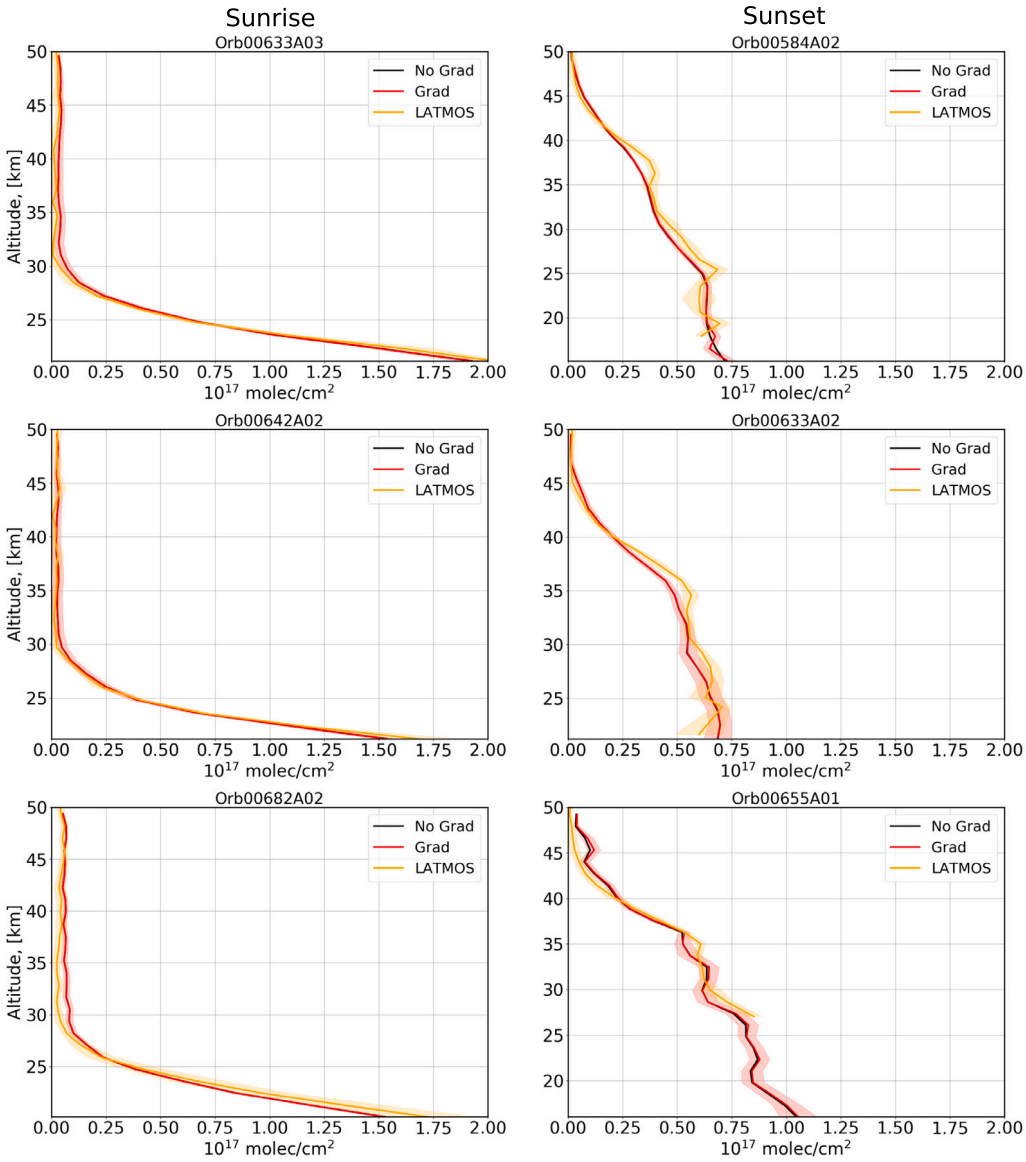

Fig. 14. Examples of retrieved ozone slant densities derived using GEM-Mars gradients (red lines) compared to profiles derived at LATMOS (orange lines). ASIMUT profile retrieved assuming a spherically symmetrical atmosphere (blue lines) are also shown. (For interpretation of the references to color in this figure legend, the reader is referred to the web version of this article.)

taken into account in the retrieval process. In the present manuscript, we applied an improved retrieval scheme that handles concentration gradients along the LOS to the retrieval of ozone from SPICAM/MEx solar occultations. We used the GEM-Mars three-dimensional General Circulation Model to quantify the input gradients across the terminator for our retrievals. Our model results strongly depend on the latitude, altitude, and season of the occultations, since ozone is affected by all these factors. Ozone does not show strong variations with solar zenith angle (local solar time) at altitudes below 25 km. Above this altitude, especially around $\sim$ 45 km near the equator, the density changes by several orders of magnitude across the terminator. In addition, near the equator, differences between sunrise and sunset variation in ozone concentration are evident and they can be explained by the ozone photochemistry. In the high latitude southern hemisphere, during the winter, ozone variations at the terminator are almost negligible.

The impact of gradients on the retrievals strongly follows the GCM model results. Uncertainties in the model ozone diurnal variations may affect the corrections to the retrieved profile. All selected sunset occultations are located near the equator while sunrise occultations are situated at high latitudes south. The sunset ozone retrieved vmr reach up to 20% difference when the asymmetry of the atmosphere is considered. At sunrise, the impact of gradients on the retrievals is negligible. This behavior can be explained by the specific location of sunrise occultations, all situated at high latitudes in the South. It is expected from the GCM model that gradients are important for sunrise retrievals near the equator.

In order to study the effects of ozone gradients at different latitudes and seasons, and in particular to investigate the differences between sunrise/sunset conditions, we plan to extend the analysis to the whole SPICAM database and to NOMAD/ExoMars observations.

Acknowledgments

The research leading to these results has received funding from the European Union's Horizon 2020 Programme (H2020-Compet-08-2014) under grant agreement UPWARDS-633127. SA is supported by the FNRS CRAMIC project under grant number T.0171.16. This project acknowledges funding by the Belgian Science Policy Office (BELSPO), with financial and contractual coordination by the ESA Prodex Office (PEA4000121493). This work was supported by the

Belgian Fonds de la Recherche Scientifique — FNRS under grant number 30442502 (ET_HOME) and through the BRAIN Research contract BR/143/A2/SCOOP.

SPICAM-UV dataset is available through the European Space Agency's Planetary Science Archive (PSA). Ozone profiles will be later available through the VESPA (Virtual European Solar and Planetary Access) interface (http://vespa.obspm.fr).

Appendix. Retrieval

The ASIMUT retrieval module is based on the use of the Optimal Estimation Method, in which *a priori* information is used to represent the best statistical knowledge of the state of the atmosphere to be retrieved, prior to any measurement. The purpose of the retrieval is then to find the approximation of the true state at the atmosphere which agrees best with both the measurement and the *a priori* information. The general forward radiative transfer equation can be written as:

$$\mathbf{y} = \mathbf{f}(\mathbf{x}, \mathbf{b}) + \epsilon \tag{A.1}$$

where $\mathbf{y}$ is the measurement vector (the measured radiance), $\mathbf{x}$ is the state vector (the vertical profiles to be retrieved), $\mathbf{b}$ represents the additional parameters used by the forward model $\mathbf{f}$, and ϵ is the random measurement noise. The forward function $\mathbf{f}$ describes the complete physics of the measurement, including the description of the instrument. $\mathbf{b}$ is a vector of model parameters (such as spectral line data, calibration parameters, etc.) that are not perfectly known by the observer. They are a possible source of random or systematic differences between calculated and measured values of $\mathbf{y}$.

In the case of a moderately nonlinear problem, the best estimate $\hat{\mathbf{x}}$ of the solution of Eq. (A.1) is found by solving iteratively

$$\mathbf{x}_{i+1} = \mathbf{x}_a + \mathbf{G}_i[\mathbf{y} - \mathbf{f}(\mathbf{x_i}) + \mathbf{K}_i(\mathbf{x}_i - \mathbf{x}_a)] \tag{A.2}$$

where x_a is the *a priori* constraint. The Jacobian matrix $\mathbf{K}$ is defined by the following expression:

$$\mathbf{K} = \frac{\partial \mathbf{f}}{\partial \mathbf{x}} \tag{A.3}$$

and the Gain matrix $\mathbf{G}$ is defined by:

$$\mathbf{G}_i = (\mathbf{S}_a^{-1} + \mathbf{K}_i^T \mathbf{S}_e^{-1} \mathbf{K}_i)^{-1} \mathbf{K}_i^T \mathbf{S}_e^{-1} \tag{A.4}$$

where $\mathbf{S}_e$ is the error covariance matrix of the measurements, and $\mathbf{S}_a$ the *a priori* covariance matrix. $\mathbf{S}_e$ is usually chosen to be diagonal, characterizing all the sources of systematic and random errors on the measured radiance.

The *a priori* covariance matrices ($\mathbf{S}_a$) represents the variability of the gas/aerosol considered. Here ASIMUT considered diagonal matrices with off-diagonal terms added as Gaussian

$$S_a(i,j) = \sqrt{S_a(i,i) S_a(j,j)} \exp\left(-\left(\frac{z_i - z_j}{l_c} \right)^2 \right) \tag{A.5}$$

to account for correlations between the concentrations at different altitudes (z_i is the altitude of level i, l_c is the vertical correlation length).

The convergence is attained when the two following conditions are met:

$$d_i^2 = (\mathbf{x}_i - \mathbf{x}_{i+1})^T \mathbf{S}^{-1} (\mathbf{x}_i - \mathbf{x}_{i+1}) \lll n \tag{A.6a}$$

$$d_i^2 = (\mathbf{f}(\mathbf{x}_{i+1}) - \mathbf{f}(\mathbf{x}_i))^T \mathbf{S}_{\delta y}^{-1} (\mathbf{f}(\mathbf{x}_{i+1}) - \mathbf{f}(\mathbf{x}_i)) \ll m \tag{A.6b}$$

with n the number of parameters to retrieve, m the number of observed points, and

$$\delta y = \mathbf{y} - \mathbf{f}(\hat{\mathbf{x}}) \tag{A.7}$$

$$\mathbf{S}_{\delta y} = \mathbf{S}_e (\mathbf{K} \mathbf{S}_a \mathbf{K}^T)^{-1} \mathbf{S}_e \tag{A.8}$$

The first expression represents the convergence condition on the fitted parameters, and the second on the difference between observed and simulated spectra.

The total error decomposes into several contributions, i.e. the smoothing error ($\mathbf{S}_{smoothing}$), the measurement error ($\mathbf{S}_{measur}$) and the forward model parameters error ($\mathbf{S}_{model}$).

$$\mathbf{S} = \mathbf{S}_{smoothing} + \mathbf{S}_{measur} + \mathbf{S}_{model} \tag{A.9}$$

In this work we have not considered the last term ($\mathbf{S}_{model}$). The measurement error propagates from the instrumental noise. Its covariance is given by:

$$\mathbf{S}_{measur} = \mathbf{G} \mathbf{S}_e \mathbf{G}^T \tag{A.10}$$

The smoothing error accounts for the sensitivity of the measurements/forward model to the variable to be retrieved (i.e. the measurement/forward model system does not allow perfectly reproducing the true atmosphere, but a smoothed value of it). The resulting error is characterized by the following covariance matrix:

$$\mathbf{S}_{smoothing} = (\mathbf{A} - \mathbf{I}) \mathbf{S}_a (\mathbf{A} - \mathbf{I})^{-1} \tag{A.11}$$

where $\mathbf{I}$ is the identity matrix, and $\mathbf{A}$ is the averaging kernel matrix. It is defined as the sensitivity of the retrieved state (hereafter symbolized by $\hat{\mathbf{x}}$) to the true state ($\mathbf{x}$) and can be calculated as:

$$\mathbf{A} = \frac{\partial \hat{\mathbf{x}}}{\partial \mathbf{x}} = \mathbf{G}\mathbf{K} \tag{A.12}$$

The rows of $\mathbf{A}$ define an averaging kernel function (AVK) for each element of $\hat{x}$, which peaks at the altitude from where most of the information is coming. In other words, the AVK provide an estimation of the vertical sensitivity of the retrieval and peak at the altitude of maximum sensitivity. The trace of the $\mathbf{A}$ matrix gives the degrees of freedom for signal (DOFS), defined as the number of independent pieces of information in the retrieved profile.

Finally the sum of these covariances associated to these different uncertainties provide an estimation of the total error on the retrieved parameters. One can show that the covariance matrix associated to $\hat{\mathbf{x}}$ is given by:

$$\mathbf{S} = (\mathbf{S}_a^{-1} + \mathbf{K}_i^T \mathbf{S}_e^{-1} \mathbf{K}_i)^{-1} \tag{A.13}$$

The square root of the diagonal elements of $\mathbf{S}$ can be seen as the error on the retrieved parameters.

References

Bertaux, J.-L., Korablev, O., Perrier, S., Quémerais, E., Montmessin, F., Leblanc, F., Lebonnois, S., Rannou, P., Lefèvre, F., Forget, F., Fedorova, A., Dimarellis, E., Reberac, A., Fonteyn, D., Chaufray, J.Y., Guibert, S., 2006. SPICAM on Mars Express: Observing modes and overview of UV spectrometer data and scientific results. J. Geophys. Res. (Planets) 111, http://dx.doi.org/10.1029/2006JE002690.

Boughner, R., Larsen, J.C., Natarajan, M., 1980. The influence of NO and CℓO variations at twilight on the interpretation of solar occultation measurements. Geophys. Res. Lett. 7, 231–234. http://dx.doi.org/10.1029/GL007i004p00231.

Brion, J., Chakir, A., Daumont, D., Malicet, J., Parisse, C., 1993. High-resolution laboratory absorption cross section of O_3. Temperature effect. Chem. Phys. Lett. 213, 610–612. http://dx.doi.org/10.1016/0009-2614(93)89169-I.

Daerden, F., Neary, L., Viscardy, S., García Muñoz, A., Clancy, R.T., Smith, M.D., Encrenaz, T., Fedorova, A., 2019. Mars atmospheric chemistry simulations with the GEM-Mars general circulation model. Icarus 326, 197–224. http://dx.doi.org/10.1016/j.icarus.2019.02.030.

Daumont, D., Brion, J., Charbonnier, J., Malicet, J., 1992. Ozone UV spectroscopy. I - Absorption cross-sections at room temperature. J. Atmos. Chem. 15, 145–155. http://dx.doi.org/10.1007/BF00053756.

Drummond, R., Vandaele, A.C., Daerden, F., Fussen, D., Mahieux, A., Neary, L., Neefs, E., Robert, S., Willame, Y., Wilquet, V., 2011. Studying methane and other trace species in the Mars atmosphere using a SOIR instrument. Planet. Space Sci. 59, 292–298. http://dx.doi.org/10.1016/j.pss.2010.05.009.

Dubovik, O., Smirnov, A., Holben, B.N., King, M.D., Kaufman, Y.J., Eck, T.F., Slutsker, I., 2000. Accuracy assessments of aerosol optical properties retrieved from Aerosol Robotic Network (AERONET) Sun and sky radiance measurements. J. Geophys. Res. 105, 9791–9806. http://dx.doi.org/10.1029/2000JD900040.

Erwin, J., Neary, L., Daerden, F., Viscardy, S., Carine Vandaele, A., 2018. Creating high-spatial resolution atmospheric profiles from the GEM-Mars GCM for the investigation of Mars. In: European Planetary Science Congress. pp. EPSC2018–717.

Forget, F., Montmessin, F., Bertaux, J.-L., González-Galindo, F., Lebonnois, S., Quémerais, E., Reberac, A., Dimarellis, E., López-Valverde, M.A., 2009. Density and temperatures of the upper Martian atmosphere measured by stellar occultations with Mars Express SPICAM. J. Geophys. Res. (Planets) 114 (13), 1004. http://dx.doi.org/10.1029/2008JE003086.

Gallery, W.O., Kneizys, F.X., Clough, S.A., 1983. Air Mass Computer Program for Atmospheric Transmittance/Radiance Calculation: FSCATM. Technical Report.

Godson, W.L., 1953. The evaluation of infra-red radiative fluxes due to atmospheric water vapour. Q. J. R. Meteorol. Soc. 79 (341), 367–379. http://dx.doi.org/10.1002/qj.49707934104.

Goody, R.M., 1952. A statistical model for water-vapour absorption. Q. J. R. Meteorol. Soc. 78 (338), 638–640. http://dx.doi.org/10.1002/qj.49707833820, URL https://rmets.onlinelibrary.wiley.com/doi/abs/10.1002/qj.49707833820, http://arxiv.org/abs/https://rmets.onlinelibrary.wiley.com/doi/pdf/10.1002/qj.49707833820.

Huestis, D.L., Berkowitz, J., 2010. Critical evaluation of the photoabsorption cross section of CO_2 from 0.125 to 201.6 nm at room temperature. In: AAS/Division for Planetary Sciences Meeting Abstracts #42. p. 48.13.

Kochenova, S., De Mazière, M., Vandaele, A., Kerzenmacher, T., Letocart, V., Kumps, N., Willame, Y., 2011. Alvl 1.0: an advanced line-by-line radiative transfer model for the retrieval of atmospheric constituents from satellite and ground-based measurements.

Lebonnois, S., Quémerais, E., Montmessin, F., Lefèvre, F., Perrier, S., Bertaux, J.-L., Forget, F., 2006. Vertical distribution of ozone on Mars as measured by SPICAM/Mars Express using stellar occultations. J. Geophys. Res. (Planets) 111, E09S05. http://dx.doi.org/10.1029/2005JE002643.

Lefèvre, F., Lebonnois, S., Montmessin, F., Forget, F., 2004. Three-dimensional modeling of ozone on Mars. J. Geophys. Res. (Planets) 109, E07004. http://dx.doi.org/10.1029/2004JE002268.

Lemoine, F.G., Neumann, G.A., Chinn, D.S., Smith, D.E., Zuber, M.T., Rowlands, D.D., Rubincam, D.P., Pavlis, D.E., 2001. Solutions for mars geophysical parameters from mars global surveyor tracking data. In: AGU Fall Meeting Abstracts. p. P42A.

Määttänen, A., Listowski, C., Montmessin, F., Maltagliati, L., Reberac, A., Joly, L., Bertaux, J.-L., 2013. A complete climatology of the aerosol vertical distribution on Mars from MEx/SPICAM UV solar occultations. Icarus 223, 892–941. http://dx.doi.org/10.1016/j.icarus.2012.12.001.

Malicet, J., Daumont, D., Charbonnier, J., Parisse, C., Chakir, A., Brion, J., 1995. Ozone UV spectroscopy. II. Absorption cross-sections and temperature dependence. J. Atmos. Chem. 21, 263–273. http://dx.doi.org/10.1007/BF00696758.

Markwardt, C.B., 2009. Non-linear Least-squares Fitting in IDL with MPFIT. In: Bohlender, D.A., Durand, D., Dowler, P. (Eds.), Astronomical Data Analysis Software and Systems XVIII. p. 251, arXiv:0902.2850.

Millour, E., Forget, F., González-Galindo, F., Spiga, A., Lebonnois, S., Montabone, L., Lewis, S.R., Read, P.L., López-Valverde, M.A., Gilli, G., Lefèvre, F., Montmessin, F., Desjean, M.C., Huot, J.P., McD/Gcm Development Team, 2008. The latest (version 4.3) mars climate database. In: Third International Workshop on the Mars Atmosphere: Modeling and Observations. p. 9029.

Mishchenko, M., Travis, L.D., 1998. Capabilities and limitations of a current FORTAN implementation of the T-matrix method for randomly oriented, rotationally symmetric scatterers. J. Quant. Spectrosc. Radiat. Transfer 60, 309–324. http://dx.doi.org/10.1016/S0022-4073(98)00008-9.

Montmessin, F., Bertaux, J.-L., Quémerais, E., Korablev, O., Rannou, P., Forget, F., Perrier, S., Fussen, D., Lebonnois, S., Rébérac, A., Dimarellis, E., 2006. Subvisible CO_2 ice clouds detected in the mesosphere of Mars. Icarus 183, 403–410. http://dx.doi.org/10.1016/j.icarus.2006.03.015.

Natarajan, M., Deaver, L.E., Thompson, E., Magill, B., 2005. Impact of twilight gradients on the retrieval of mesospheric ozone from HALOE. J. Geophys. Res. (Atmos.) 110, D13305. http://dx.doi.org/10.1029/2004JD005719.

Neary, L., Daerden, F., 2018. The GEM-Mars general circulation model for Mars: Description and evaluation. Icarus 300, 458–476. http://dx.doi.org/10.1016/j.icarus.2017.09.028.

Nevejans, D., Neefs, E., van Ransbeeck, E., Berkenbosch, S., Clairquin, R., de Vos, L., Moelans, W., Glorieux, S., Baeke, A., Korablev, O., Vinogradov, I., Kalinnikov, Y., Bach, B., Dubois, J.-P., Villard, E., 2006. Compact high-resolution spaceborne echelle grating spectrometer with acousto-optical tunable filter based order sorting for the infrared domain from 2.2 to 4.3 μm. Appl. Opt. 45, 5191–5206. http://dx.doi.org/10.1364/AO.45.005191.

O'Neill, N., Royer, A., 1993. Extraction of bimodal aerosol-size distribution radii from spectral and angular slope (Angstrom) coefficients. Appl. Opt. 32, 1642–1645. http://dx.doi.org/10.1364/AO.32.001642.

Parkinson, W.H., Rufus, J., Yoshino, K., 2003. Absolute absorption cross section measurements of CO_2 in the wavelength region 163-200 nm and the temperature dependence. Chem. Phys. 290, 251–256. http://dx.doi.org/10.1016/S0301-0104(03)00146-0.

Quémerais, E., Bertaux, J.-L., Korablev, O., Dimarellis, E., Cot, C., Sandel, B.R., Fussen, D., 2006. Stellar occultations observed by SPICAM on Mars Express. J. Geophys. Res. (Planets) 111, 9. http://dx.doi.org/10.1029/2005JE002604.

Robert, S., Camy-Peyret, C., Daerden, F., De Mazière, M., De Wachter, E., Neary, L., Vandenbussche, S., Vandaele, A.C., 2017. Two test-cases for synergistic detections in the Martian atmosphere: Carbon monoxide and methane. J. Quant. Spectrosc. Radiat. Transfer 189, 86–104. http://dx.doi.org/10.1016/j.jqsrt.2016.11.003.

Robert, S., Vandaele, A.C., Thomas, I., Willame, Y., Daerden, F., Delanoye, S., Depiesse, C., Drummond, R., Neefs, E., Neary, L., Ristic, B., Mason, J., Lopez-Moreno, J.J., Rodriguez- Gomez, J., Patel, M.R., Bellucci, G., Vandaele, A.C., Lopez Moreno, J.J., Bellucci, G., Patel, M., Allen, M., Altieri, F., Aoki, S., Bolsée, D., Clancy, T., Cloutis, E., Daerden, F., Depiesse, C., Fedorova, A., Formisano, V., Funke, B., Fussen, D., Garcia- Comas, M., Geminale, A., Gérard, J.C., Gillotay, D., Giuranna, M., Gonzalez-Galindo, F., Ignatiev, N., Kaminski, J., Karatekin, O., Kasaba, Y., Lefèvre, F., Lewis, S., Ló pez-Puertas, M., López-Valverde, M., Mahieux, A., Mason, J., McConnell, J., Mumma, M., Neary, L., Neefs, E., Novak, R., Renotte, E., Robert, S., Sindoni, G., Smith, M., Thomas, I.R., Trokhimovskiy, A., Vander Auwera, J., Villanueva, G., Viscardy, S., Whiteway, J., Willame, Y., Wilquet, V., Wolff, M., Alonso- Rodrigo, G., Aparicio del Moral, B., Barzin, P., BenMoussa, A., Berkenbosch, S., Biondi, D., Bonnewijn, S., Candini, G., Clairquin, R., Cubas, J., Delanoye, S., Giordanengo, B., Gissot, S., Gomez, A., Zafra, J.J., Leese, M., Maes, J., Mazy, E., Mazzoli, A., Meseguer, J., Morales, R., Orban, A., Pastor-Morales, M., Perez-Grande, I., Ristic, B., Rodriguez-Gomez, J., Saggin, B., Samain, V., Sanz Andres, A., Sanz, R., Simar, J.F., Thibert, T., NOMAD Team, 2016. Expected performances of the NOMAD/ExoMars instrument. Planet. Space Sci. 124, 94–104. http://dx.doi.org/10.1016/j.pss.2016.03.003.

Rodgers, C.D., 2000. Inverse methods for atmospheric sounding: Theory and practice. http://dx.doi.org/10.1142/3171.

Sander, S.P., Abbatt, J., Barker, J., Burkholder, J., Friedl, R., Golden, D., Huie, R., Kolb, C., Kurylo, M., Moortgat, G., Orkin, V., Wine, P., 2011. Chemical kinetics and photochemical data for use in atmospheric studies.

Serdyuchenko, A., Gorshelev, V., Weber, M., Chehade, W., Burrows, J.P., 2014. High spectral resolution ozone absorption cross-sections - Part 2: Temperature dependence. Atmos. Meas. Tech. 7, 625–636. http://dx.doi.org/10.5194/amt-7-625-2014.

Smith, D.E., Zuber, M.T., Solomon, S.C., Phillips, R.J., Head, J.W., Garvin, J.B., Banerdt, W.B., Muhleman, D.O., Pettengill, G.H., Neumann, G.A., Lemoine, F.G., Abshire, J.B., Aharonson, O., Brown, C., Hauck, S.A., Ivanov, A.B., McGovern, P.J., Zwally, H.J., Duxbury, T.C., 1999. The global topography of mars and implications for surface evolution. Science 284, 1495. http://dx.doi.org/10.1126/science.284.5419.1495.

Sneep, M., Ubachs, W., 2005. Direct measurement of the Rayleigh scattering cross section in various gases. J. Quant. Spectrosc. Radiat. Transfer 92, 293–310. http://dx.doi.org/10.1016/j.jqsrt.2004.07.025.

Spurr, R.J.D., 2006. VLIDORT: A linearized pseudo-spherical vector discrete ordinate radiative transfer code for forward model and retrieval studies in multilayer multiple scattering media. J. Quant. Spectrosc. Radiat. Transfer 102, 316–342. http://dx.doi.org/10.1016/j.jqsrt.2006.05.005.

Trompet, L., Mahieux, A., Ristic, B., Robert, S., Wilquet, V., Thomas, I.R., Vandaele, A.C., Bertaux, J.-L., 2016. Improved algorithm for the transmittance estimation of spectra obtained with SOIR/Venus Express. Appl. Opt. 55, 9275. http://dx.doi.org/10.1364/AO.55.009275.

Vandaele, A.C., De Mazière, M., Drummond, R., Mahieux, A., Neefs, E., Wilquet, V., Korablev, O., Fedorova, A., Belyaev, D., Montmessin, F., Bertaux, J.L., 2008. Composition of the Venus mesosphere measured by Solar Occultation at Infrared on board Venus Express. J. Geophys. Res. (Planets) 113, E00B23. http://dx.doi.org/10.1029/2008JE003140.

Vandaele, A.C., Kruglanski, M., de Mazière, M., 2006. Modeling and retrieval of atmospheric spectra using ASIMUT. In: Atmospheric Science Conference. p. 71.

Vandaele, A.C., Lopez-Moreno, J.J., Patel, M.R., Bellucci, G., Daerden, F., Ristic, B., Robert, S., Thomas, I.R., Wilquet, V., Allen, M., Alonso-Rodrigo, G., Altieri, F., Aoki, S., Bolsée, D., Clancy, T., Cloutis, E., Depiesse, C., Drummond, R., Fedorova, A., Formisano, V., Funke, B., González-Galindo, F., Geminale, A., Gérard, J.C., Giuranna, M., Hetey, L., Ignatiev, N., Kaminski, J., Karatekin, O., Kasaba, Y., Leese, M., Lefèvre, F., Lewis, S.R., López-Puertas, M., López-Valverde, M., Mahieux, A., Mason, J., McConnell, J., Mumma, M., Neary, L., Neefs, E., Renotte, E., Rodriguez-Gomez, J., Sindoni, G., Smith, M., Stiepen, A., Trokhimovsky, A., Vander Auwera, J., Villanueva, G., Viscardy, S., Whiteway, J., Willame, Y., Wolff, M., 2018. NOMAD, an integrated suite of three spectrometers for the exomars trace gas mission: Technical description, science objectives and expected performance. SSR 214, 80. http://dx.doi.org/10.1007/s11214-018-0517-2.

Vandaele, A.C., Mahieux, A., Robert, S., Berkenbosch, S., Clairquin, R., Drummond, R., Letocart, V., Neefs, E., Ristic, B., Wilquet, V., Colomer, F., Belyaev, D., Bertaux, J.-L., 2013. Improved calibration of SOIR/Venus Express spectra. Opt. Express 21, 21148. http://dx.doi.org/10.1364/OE.21.021148.

Vandenbussche, S., Kochenova, S., Vandaele, A.C., Kumps, N., De Mazière, M., 2013. Retrieval of desert dust aerosol vertical profiles from IASI measurements in the TIR atmospheric window. Atmos. Meas. Tech. 6, 2577–2591. http://dx.doi.org/10.5194/amt-6-2577-2013.

Willame, Y., Vandaele, A.C., Depiesse, C., Lefèvre, F., Letocart, V., Gillotay, D., Montmessin, F., 2017. Retrieving cloud, dust and ozone abundances in the Martian atmosphere using SPICAM/UV nadir spectra. Planet. Space Sci. 142, 9–25. http://dx.doi.org/10.1016/j.pss.2017.04.011.